# 3D Clifford Analytic Signal for 3D Envelope Detection on Ultrasound Volume

Liang Wang, Patrick R Girard, Patrick Clarysse, Philippe Delachartre

# 3D Clifford Analytic Signal for 3D Envelope Detection on Ultrasound Volume

Liang Wang
Univ Lyon, INSA-LYON, Université Claude Bernard Lyon 1, UJM-Saint Etienne, CNRS, Inserm, CREATIS UMR 5220, U1206, 69621, Lyon, France
liang.wang@hotmail.fr

Patrick R. Girard
Univ Lyon, INSA-LYON, Université Claude Bernard Lyon 1, UJM-Saint Etienne, CNRS, Inserm, CREATIS UMR 5220, U1206, 69621, Lyon, France
patrick.girard@insa-lyon.fr

Patrick Clarysse
Univ Lyon, INSA-LYON, Université Claude Bernard Lyon 1, UJM-Saint Etienne, CNRS, Inserm, CREATIS UMR 5220, U1206, 69621, Lyon, France
patrick.clarysse@creatis.insa-lyon.fr

Philippe Delachartre
Univ Lyon, INSA-LYON, Université Claude Bernard Lyon 1, UJM-Saint Etienne, CNRS, Inserm, CREATIS UMR 5220, U1206, 69621, Lyon, France
philippe.delachartre@creatis.insa-lyon.fr

***Abstract*—Envelope detection is one of the essential steps for ultrasound B-mode image reconstruction. Typically, this reconstruction is based on one dimensional (1D) radio frequency (RF) signal demodulation. In the literature, 1D envelopes are usually stacked to achieve two or three dimensional (2D or 3D) envelope detection, which leads to possible losses of multi-dimensional context information. In this paper, we propose a hypercomplex analytical signal in the form of Clifford biquaternion, which is called 3D Clifford analytic signal (3D CAS). Firstly, the convolution is utilized to define the 3D CAS in terms of biquaternion. Next, the relation between the 3D CAS and the classical Hahn's analytical signals in the 3D case is illustrated with the help of Hilbert transforms, which enables a reliable numerical implementation of 3D CAS. Then, the modulus of 3D CAS is proposed and applied to a straightforward 3D ultrasonic RF envelope detection by taking into consideration the information of amplitude of all three directions of space. Experiments were carried out on the ultrasound volume from a phantom with a biopsy needle inserted. The experiments provide a better visual experience from envelope images of RF volume than the compared 1D and 2D methods. The 3D and 2D envelopes present 36.5% and 15.2% improvement to 1D, respectively, from the contrast to noise ratio between the needle region and the adjacent background. From an independent public 2D liver tumor RF sequences of 29 mice, the average structural index similarity (SSIM) and peak signal to noise ratio (PSNR) were improved by 53.0% and 39.0%, respectively, from 2D envelopes comparing to 1D envelopes.**

***Index Terms*—3D Clifford analytic signal, Clifford biquaternion, hypercomplex analytical signal, Ultrasound imaging**

## I. Introduction

It is well known that the analytic signal (AS) is able to split a signal into local phase and local amplitude [1]. Different definitions of the complex and hypercomplex analytical signal are proposed for applications of signal and image processing [2], [3]. In the medical image processing domain, the local phase is also widely used in, for example, 2D and 3D ultrasound image registration [4], motion estimation [5], etc. The envelope of the ultrasonic RF signal can be computed from the instantaneous amplitude of the AS. Traditionally in 1D case, only one type of AS can be defined, which is to define the input ultrasonic RF signal and its Hilbert transform are defined as the real part and imaginary part, respectively, in a 1D AS [6]. In the 2D case, several definitions of AS are proposed and they provide their own instantaneous amplitudes differently for 2D envelope detection. For example, two instantaneous amplitudes should be considered in Hahn's 2D single-quadrant complex signal [3] for a full envelope reconstruction. Three definitions of 2D quaternion signal (QS) can be obtained based on the two-side, left-side, and right-side quaternion Fourier transformation (QFT), respectively [7]. They lead to three ways of instantaneous amplitude calculation. Moreover, 2D monogenic signal is also adopted for 2D envelope detection [6]. In the 3D case, several state-of-the-art work adopted 1D RF scan line in the envelope detection step, without taking care of the spatial relation between 1D scan lines in the second and third dimension [8], [9].

Generally, without taking into account all the 3D spatial relations of the signal, both of the above 1D or 2D AS-based methods may bring potential loss of information during the full 3D envelope detection processing. Moreover, it is difficult to find a uniform manner for multi-dimensional signal envelope detection in 1D, 2D, and 3D cases. In this paper, we propose a 3D CAS within the Clifford algebra framework. The convolution form is utilized for the signal definition instead of using the Fourier transformation form in this work. The advantage of the definition in convolution form is that allows us to extend the definition from 1D and 2D to 3D case with a unique form.

Furthermore, we use the convolution form to represent Hahn's 2D single-quadrant complex signal in a 3D case and deduced that it has a linear relation with the proposed 3D CAS based on the Hilbert transform. Finally, the modulus of the proposed 3D CAS is presented. Experiments were carried out on the private ultrasound volume data from a phantom with

a biopsy needle inserted. Moreover, an independent public 2D liver tumor RF sequences of 29 mice were used for evaluation [10]. Advantages of 3D CAS were shown for RF ultrasound volume processing from these experiments.

## II. 3D Hahn single-orthant AS

The theory of complex signals was extended to nD by Hahn et al. [3] in 2011. In this paper, we would call the 3D Hahn single-orthant AS as 3D Hahn AS for short. The Hermitian symmetry, which is one property of 3D Fourier transform in 3D case, is applied to calculate the 3D Hahn AS. As shown in Fig. 1, the 3D frequency space has eight ($2^3$) orthants. Based on the Hermitian symmetry of the Fourier transformation, that the input signal can be recovered from any of its half plane spectrum, the 3D real signal can be represented by four ($2^3/2$) analytic signals. In the following, without loss of generality, we work on the half space spectra with $u > 0$ to calculate the four single-orthant analytic signals, that is to say the orthants with the labels I, III, V, and VII in Fig. 1. By the definition in [3], we can obtain four Hahn AS ($\psi_1, \psi_3, \psi_5$, and $\psi_7$) from the orthants I, III, V, and VII, respectively, from a 3D real signal $f(x, y, z)$. Hence, we have:

$$\psi_n(x,y,z) = f(x,y,z) \star\star\star \left\{ \left[\delta(x) + s_u s_v s_w \frac{i}{\pi x}\right] \left[\delta(y) + s_u s_v s_w \frac{i}{\pi y}\right] \left[\delta(z) + s_u s_v s_w \frac{i}{\pi z}\right] \right\}, \quad (1)$$

where $n = 1, 3, 5, 7$, $\star\star\star$ is the 3D convolution. $s_u$, $s_v$, and $s_w$ are the sign function for axes $u$, $v$, and $w$ in Fig. 1, respectively. When developing $\psi_1(x, y, z)$, we have:

$$\begin{aligned}
&\psi_1(x,y,z) = \\
&f(x,y,z) \star\star\star \left\{ \delta(x)\delta(y)\delta(z) + i\frac{\delta(x)\delta(y)}{\pi z} + i\frac{\delta(x)\delta(z)}{\pi y} \right. \\
&\left. -\frac{\delta(x)}{\pi^2 yz} + i\frac{\delta(y)\delta(z)}{\pi x} - \frac{\delta(y)}{\pi^2 xz} - \frac{\delta(z)}{\pi^2 xy} - i\frac{1}{\pi^3 xyz} \right\} \\
&= (f - H_{xy}\{f\} - H_{xz}\{f\} - H_{yz}\{f\}) + i\,(H_x\{f\} \\
&+ H_y\{f\} + H_z\{f\} - H\{f\}) = a_1 \cos\varphi_1 + i a_1 \sin\varphi_1, \quad (2)
\end{aligned}$$

where $H\{f\}$ is the total Hilbert transform of $f(x, y, z)$, and $H_x\{f\}, H_y\{f\}, H_z\{f\}$ are the partial Hilbert transforms for one direction $x$,$y$ and $z$ of $f(x, y, z)$, separately, and $H_{xy}\{f\}, H_{yz}\{f\}, H_{xz}\{f\}$ are the partial Hilbert transforms for two directions $(x, y)$, $(y, z)$, and $(x, z)$ of $f(x, y, z)$, separately. $a_1$ and $\varphi_1$ are the modulus and the phase, respectively, of the polar form of $\psi_1$. Similarly, the 3D Hahn AS from the third, fifth and seventh orthant of Fourier spectra are, respectively:

$$\begin{aligned}
&\psi_3(x,y,z) = (f + H_{xy}\{f\} - H_{xz}\{f\} + H_{yz}\{f\}) + i\,(H_x\{f\} \\
&-H_y\{f\} + H_z\{f\} + H\{f\}) = a_3 \cos\varphi_3 + i a_3 \sin\varphi_3, \quad (3) \\
&\psi_5(x,y,z) = (f - H_{xy}\{f\} + H_{xz}\{f\} + H_{yz}\{f\}) + i\,(H_x\{f\} \\
&+H_y\{f\} - H_z\{f\} + H\{f\}) = a_5 \cos\varphi_5 + i a_5 \sin\varphi_5, \quad (4) \\
&\psi_7(x,y,z) = (f + H_{xy}\{f\} + H_{xz}\{f\} - H_{yz}\{f\}) + i\,(H_x\{f\} \\
&-H_y\{f\} - H_z\{f\} - H\{f\}) = a_7 \cos\varphi_7 + i a_7 \sin\varphi_7. \quad (5)
\end{aligned}$$

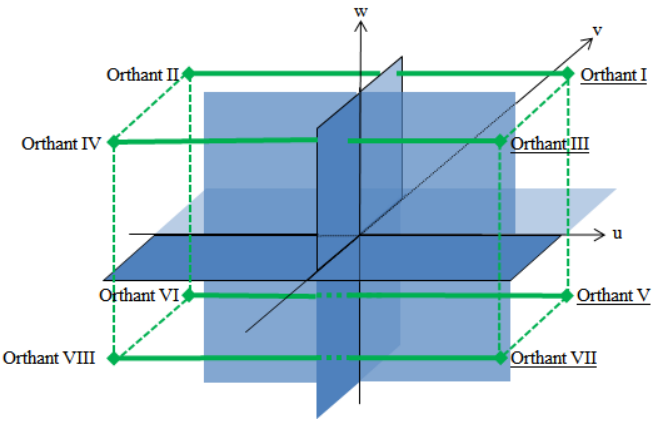


Fig. 1. The eight orthants frequency space with a label number of each orthant. $u, v, w$ are the spatial frequencies.

Equations (2)-(5) illustrate that the four 3D Hahn ASs can be represented by the 3D Hilbert transforms of the input signal. Further, the 3D Hilbert transforms can be recovered by the phases and modulus of its 3D Hahn ASs. These properties are adopted in the next section.

## III. 3D Clifford analytic signal

In [3], it is proved that the 2D hypercomplex quaternion signal can be recovered by classical complex 2D Hahn ASs. Inspired by this idea, we propose the 3D CAS by taking the framework of 3D Clifford algebra (with three generators). Then we deduce a relation between 3D hypercomplex Hahn AS signal and the 3D complex signal, which help to define and implement the modulus of the 3D CAS.

### A. Definition of 3D CAS in Clifford biquaternion form

In order to extend the notion of AS to the 3D case with the Clifford algebra, the Clifford biquaternions could be considered [11], which have three generators as $e_1, e_2, e_3$. The full algebra contains eight elements:

$$\begin{bmatrix} 1, & i = e_2e_3, & j = e_3e_1, & k = e_1e_2, \\ \epsilon = -e_1e_2e_3, & \epsilon i = e_1, & \epsilon j = e_2, & \epsilon k = e_3 \end{bmatrix}, \quad (6)$$

with $\epsilon^2 = 1, e_1^2 = e_2^2 = e_3^2 = -1$. For a 3D input real signal $f(x, y, z)$, the 3D CAS $\psi_{cas}(x, y, z)$ can be defined as below in Clifford biquaternion form:

$$\psi_{cas}(x,y,z) = \quad (7)$$
$$f(x,y,z) \star\star\star \left\{ \left[\delta(x) + \frac{e_1}{\pi x}\right] \left[\delta(y) + \frac{e_2}{\pi y}\right] \left[\delta(z) + \frac{e_3}{\pi z}\right] \right\}.$$

From (6) and (7), one obtains:

$$\begin{aligned}
\psi_{cas}(x,y,z) &= f + iH_{yz}\{f\} + j(-H_{xz}\{f\}) + kH_{xy}\{f\} \\
&+ \epsilon(-H\{f\}) + \epsilon i H_x\{f\} + \epsilon j H_y\{f\} + \epsilon k H_z\{f\}, \quad (8)
\end{aligned}$$

where $e_1, e_2, e_3$ are the imaginary units with the relation in (6). All the eight elements constitute a biquaternion.

### B. Expression of the 3D CAS in terms of 3D Hahn ASs

From (8) and section II, it is found that all the elements in both of the 3D Hahn AS and 3D CAS can be represented by the total and partial Hilbert Transform of the original real signal, except that their imaginary units are different. Therefore, to substitute the 3D Hahn AS polar form results from Eqs. (2)-(5) to 3D CAS $\psi_{cas}$ in (8), we obtain the 3D CAS that represented by the modulus and phases of 3D Hahn single-quadrant AS as follows:

$$\begin{aligned}\psi_{cas} = \quad & (9)\\ & \frac{1}{4}[(a_1\cos\varphi_1 + a_3\cos\varphi_3 + a_5\cos\varphi_5 + a_7\cos\varphi_7)\\ & + i\,(-a_1\cos\varphi_1 + a_3\cos\varphi_3 + a_5\cos\varphi_5 - a_7\cos\varphi_7)\\ & + j\,(a_1\cos\varphi_1 + a_3\cos\varphi_3 - a_5\cos\varphi_5 - a_7\cos\varphi_7)\\ & + k\,(-a_1\cos\varphi_1 + a_3\cos\varphi_3 - a_5\cos\varphi_5 + a_7\cos\varphi_7)\\ & + \epsilon\,(a_1\sin\varphi_1 - a_3\sin\varphi_3 - a_5\sin\varphi_5 + a_7\sin\varphi_7)\\ & + \epsilon i\,(a_1\sin\varphi_1 + a_3\sin\varphi_3 + a_5\sin\varphi_5 + a_7\sin\varphi_7)\\ & + \epsilon j\,(a_1\sin\varphi_1 - a_3\sin\varphi_3 + a_5\sin\varphi_5 - a_7\sin\varphi_7)\\ & + \epsilon k\,(a_1\sin\varphi_1 + a_3\sin\varphi_3 - a_5\sin\varphi_5 - a_7\sin\varphi_7)].\end{aligned}$$

Using the biquaternion product and the biquaternion conjugate defined in [11], one obtains the property: $\psi_{cas}(\psi_{cas})_c = \frac{1}{4}[a_1^2+a_3^2+a_5^2+a_7^2]+\epsilon\frac{1}{2}[a_1a_3\sin(\varphi_1-\varphi_3)-a_5a_7\sin(\varphi_5-\varphi_7)]$ where $(\psi_{cas})_c$ is the biquaternion conjugate of $\psi_{cas}$. Let $\psi_{cas} = |\psi_{cas}|e^{\epsilon\phi}a$, where $|\psi_{cas}|$ is the modulus for $\psi_{cas}$, $a$ is the unit biquaternion. One obtains: $\psi_{cas}(\psi_{cas})_c = |\psi_{cas}|^2e^{2\epsilon\phi} = |\psi_{cas}|^2[ch(2\phi)+\epsilon sh(2\phi)]$, with $ch(\cdot)$ and $sh(\cdot)$ the hyperbolic cosine and sine function, respectively. Hence, we can define $\psi_{cas}(\psi_{cas})_c = A+\epsilon B$, with $A = |\psi_{cas}|^2ch(2\phi), B = |\psi_{cas}|^2sh(2\phi)$, where $A$ and $B$ is the scalar part and pseudo-scalar part of the biquaternion $\psi_{cas}(\psi_{cas})_c$. Then, $A^2-B^2 = |\psi_{cas}|^4[ch(2\phi)^2-sh(2\phi)^2] = |\psi_{cas}|^4$. Therefore, we have: $|\psi_{cas}| = \sqrt[4]{A^2-B^2}$. As the result, the modulus $|\psi_{cas}|$ of $\psi_{cas}$ can be obtained as below:

$$|\psi_{cas}| = \left\{\left[\frac{a_1^2+a_3^2+a_5^2+a_7^2}{4}\right]^2 - \left[\frac{a_1a_3\sin(\varphi_1-\varphi_3)-a_5a_7\sin(\varphi_5-\varphi_7)}{2}\right]^2\right\}^{\frac{1}{4}}, \quad (10)$$

which can be employed to calculate the modulus of a 3D input signal as an application. In addition, $|\psi_{cas}|$ is a general modulus form for 1D Hahn AS and 2D QS. For a 1D input signal, $a_1 = a_3 = a_5 = a_7$, and $\varphi_1 = \varphi_3 = \varphi_5 = \varphi_7$ , respectively, in (10), then $|\psi_{cas}| = a_1$. For a 2D input signal, $a_1 = a_5, a_3 = a_7$, and $\varphi_1 = \varphi_5, \varphi_3 = \varphi_7$, respectively, in (10), then $|\psi_{cas}| = \sqrt{\frac{a_1^2+a_3^2}{2}}$. They are equivalent to the work in [3].

## IV. Experiments: Application of 3D envelope detection by 3D CAS

The 3D CAS of the RF ultrasound volume is constructed with the ultrasound imaging platform at CREATIS Laboratory.

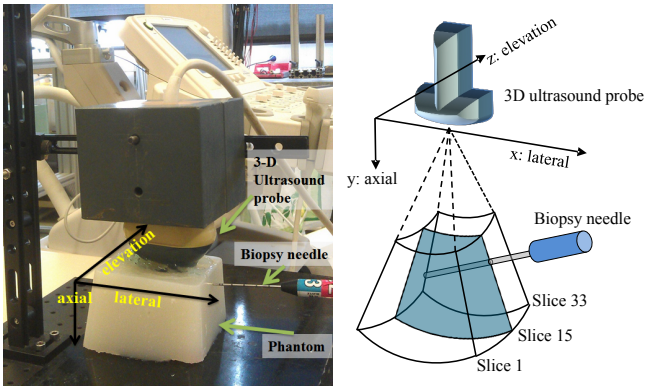


(a) (b)

Fig. 2. (a) RF ultrasound volume acquisition platform with a biopsy needle in a homemade agar ultrasound phantom. (b) An illustration of the experimental platform.

The acquisition of the volume was carried out using an Ultrasonix MDP scanner and an ultrasound linear probe 4D motorized abdominal transducer: 4DC7-3/40 (Ultrasonix) with a 40-MHz sampling frequency. Then the modulus $|\psi_{cas}(x,y,z)|$ of (10) of the 3D CAS is used as an envelope of the ultrasound volume. As shown in Fig. 2(a), a biopsy needle was inserted into a homemade agar ultrasound phantom.

The acquired data was 33 slices with a field of view was 45.6°. Figure 2(b) illustrates the numerical calculation that corresponds to the acquisition platform of the ultrasound volume data in Fig. 2(a). The biopsy needle is inserted into a plane around the middle of the 3D ultrasound volume around $z$-direction slice 15. We compared the 3D CAS envelope results with the 1D Hahn AS and 2D classical QS envelope detection results as showed in Fig. 3. To compare the results under the same reference, the gray value of the slice images was normalized between the minimum and maximum values of all three types of data for all the envelope slices. One slice of the total 33 slices along the elevation direction is presented. On slice 15 along the $z$-direction, the profile on the envelope image of the 3D CAS shows the biopsy needle structure more clearly. The vertical profiles of the envelope from the 1D, 2D, and 3D methods are presented in Fig. 3(d). Moreover, the parallelograms in Fig. 3(a)-(c) indicate the position of the biopsy needle. In the parallelogram region, the profiles along the direction of the biopsy needle axis are presented in Fig. 3(e). From these profiles, the 3D CAS envelope result shows a contrast optimization compared with 1D and 2D envelope results. Generally, the 3D and 2D envelopes present 36.5% and 15.2% improvement to 1D, respectively, from the contrast to noise ratio between the needle region and the adjacent background. In addition, from an independent public 2D liver tumor RF sequences of 29 mice [10]. An example of this dataset (case "Cage04_B_loc") was shown in Fig. 4. All the envelopes were normalized under the same scale. According to the ground truth tumor region indicated in red color in Fig. 4(d), better visual experiences could be obtained from the edge of the tumor region in 2D (Fig. 4(b)) and

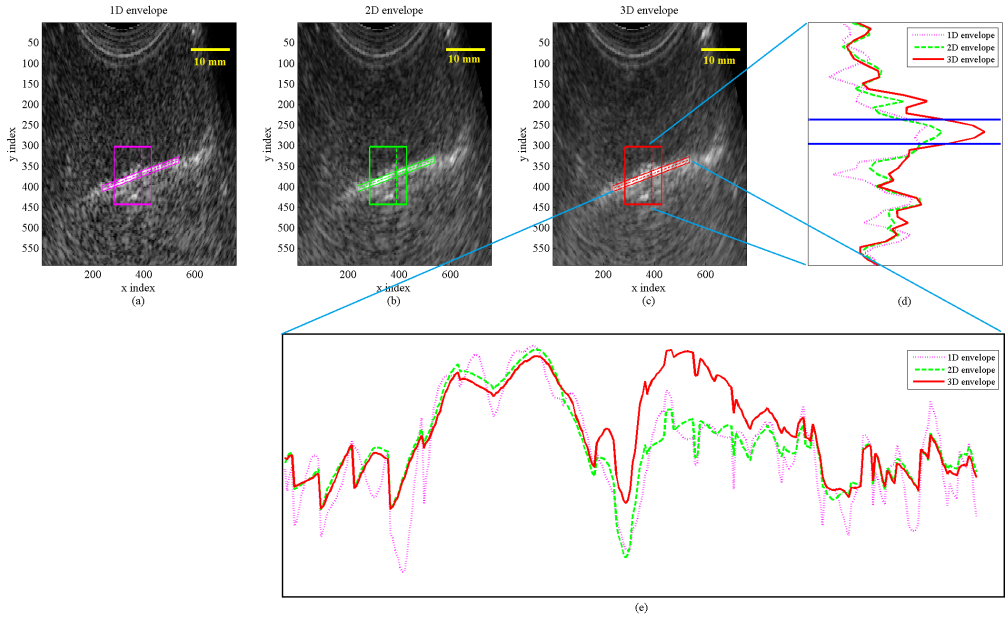


Fig. 3. RF ultrasound filtered envelope comparison of a slice in elevation direction: (a) 1D Hahn envelope; (b) 2D QS envelope (based on two-side QFT); (c) 3D CAS; (d) three vertical profiles of 1D, 2D, and 3D envelope in the same position; (e) three profiles along the biopsy needle axis of 1D, 2D, and 3D envelope at the same position.

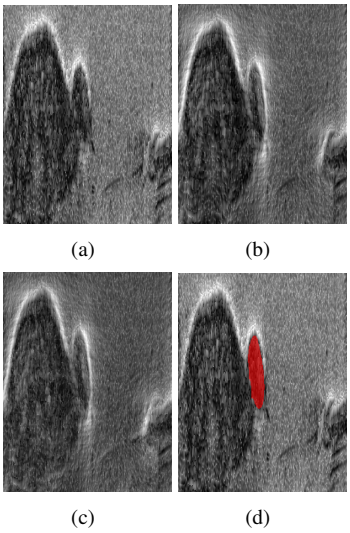


Fig. 4. Reconstructed B-mode image from (a) 1D, (b) 2D, and (c) 3D envelopes with (d) ground truth tumor region (in red) on 1D envelope.

3D (Fig. 4(c)) envelopes than the one in the 1D envelope (Fig. 4(a)). In addition, the 2D and 3D envelopes show a lower amplitude of noise from the background region in Fig. 4(b) and (c) than the 1D envelope in Fig. 4(a). From the whole dataset of 29 mice, the average SSIM and PSNR of reconstructed B-mode image were improved by 53.0% and 39.0% from 2D envelopes comparing to 1D envelopes, respectively.

## V. Conclusion

The 3D CAS is proposed in this work firstly, which is defined based on an extension of convolution form of 1D AS definition in the framework of Clifford algebra. Next, the relation between the 3D CAS and four single-orthant 3D Hahn ASs is discussed. Then, a straightforward relation was established between them by the total and partial Hilbert transform of the input signal. The 3D CAS modulus is defined and applied for a 3D envelope detection of a RF ultrasound volume. The results demonstrate that the 3D CAS has advantages for RF ultrasound volume processing. We calculated the 1D, 2D, and 3D envelopes for a RF ultrasound volume that was acquired from an ultrasound phantom with a biopsy needle inserted. Comparing the three types of envelope results, the 3D CAS envelope gives a more precise local feature image of the biopsy needle. This potentially improves the quality for applications such as object detection, 3D segmentation and registration, etc.

## References

[1] S. J. Sangwine and N. Le Bihan, "Hypercomplex analytic signals: extension of the analytic signal concept to complex signals," in *Proceedings of the 15th European Signal Processing Conference*, Poznan, Pologne, 2007, pp. 621–624.

[2] M. Felsberg, "Optical flow estimation from monogenic phase," in *Complex Motion*, ser. Lecture Notes in Computer Science, B. Jähne, R. Mester, E. Barth, and H. Scharr, Eds. Springer Berlin Heidelberg, Jan 2007, no. 3417, pp. 1–13.

[3] S. Hahn and K. Snopek, "The unified theory of n-dimensional complex and hypercomplex analytic signals," *Bulletin of the Polish Academy of Sciences: Technical Sciences*, vol. 59, no. 2, pp. 167–181, 2011.

[4] D. Lee, W. H. Nam, J. Y. Lee, and J. B. Ra, "Non-rigid registration between 3D ultrasound and CT images of the liver based on intensity and gradient information," *Physics in Medicine and Biology*, vol. 56, no. 1, pp. 117–137, 2011.

[5] L. Wang, A. Basarab, P. R. Girard, P. Croisille, P. Clarysse, and P. Delachartre, "Analytic signal phase-based myocardial motion estimation in tagged mri sequences by a bilinear model and motion compensation," *Medical Image Analysis*, vol. 24, no. 1, pp. 149–162, Jun 2015.

[6] C. Wachinger, T. Klein, and N. Navab, "The 2D analytic signal for envelope detection and feature extraction on ultrasound images," *Medical Image Analysis*, vol. 16, no. 6, pp. 1073–1084, Aug 2012.

[7] S.-C. Pei, J.-J. Ding, and J.-H. Chang, "Efficient implementation of quaternion fourier transform, convolution, and correlation by 2-D complex FFT," *IEEE Transactions on Signal Processing*, vol. 49, no. 11, pp. 2783–2797, Nov 2001.

[8] J. Du, X.-L. Mao, P.-F. Ye, and Q.-H. Huang, "Three-dimensional reconstruction and visualization of human enamel ex vivo using high-frequency ultrasound," *Journal of Medical and Biological Engineering*, vol. 37, no. 1, pp. 112–122, Feb 2017.

[9] C. Li, J. Yang, X. Li, X. Zhong, J. Song, M. Ding, and M. Yuchi, "Real-time 3D image reconstruction of a 24 × 24 row-column addressing array: from raw data to image," in *Medical Imaging 2016: Ultrasonic Imaging and Tomography*, Apr 2016, pp. 9790–9790–6.

[10] O. S. Al-Kadi, D. Y. Chung, R. C. Carlisle, C. C. Coussios, and J. A. Noble, "Quantification of ultrasonic texture intra-heterogeneity via volumetric stochastic modeling for tissue characterization," *Medical Image Analysis*, vol. 21, no. 1, pp. 59–71, 2015.

[11] P. Girard, R. Pujol, P. Clarysse, A. Marion, R. Goutte, and P. Delachartre, "Analytic video (2D + t) signals using Clifford-Fourier transforms in multiquaternion Grassmann Hamilton Clifford algebras," in *Quaternion and Clifford Fourier Transforms and Wavelets*, ser. Trends in Mathematics, E. Hitzer and S. J. Sangwine, Eds. Springer Basel, 2013, pp. 197–219.